Self-Referenced Spectral Interferometry for Single-Shot Characterization of Ultrashort Free-Electron Laser Pulses

Yaozong Xiao,[1,2,3] Hao Sun,[4] Bo Liu,[1,3] Zhentang Zhao,[1,3] and Chao Feng[1,3,*]
[1]Shanghai Institute of Applied Physics, Chinese Academy of Sciences, Shanghai 201800, China
[2]University of Chinese Academy of Sciences, Beijing 100049, China
[3]Shanghai Advanced Research Institute, Chinese Academy of Sciences, Shanghai 201210, China
[4]Institute of Advanced Science Facilities, Shenzhen 518107, China

(Received 10 March 2023; revised 17 June 2023; accepted 18 October 2023; published 14 November 2023)

An attosecond x-ray pulse with known spectrotemporal information is an essential tool for the investigation of ultrafast electron dynamics in quantum systems. Ultrafast free-electron lasers (FELs) have the unique advantage on unprecedented high intensity at x-ray wavelengths. However, no suitable method has been established so far for the spectrotemporal characterization of these ultrashort x-ray pulses. In this Letter, a simple method has been proposed based on self-referenced spectral interferometry for reconstructing the temporal profile and phase of ultrashort FEL pulses. We have demonstrated that the proposed method is reliable to completely characterize the attosecond x-ray FEL pulses with an error at the level of a few percent. Moreover, the first proof-of-principle experiment has been performed to achieve the single-shot spectrotemporal characterization of ultrashort pulses from a high-gain FEL. The precision of the proposed method will be enhanced with the decrease of the pulse duration, paving a new way for complete attosecond pulse characterization at x-ray FELs.

DOI: 10.1103/PhysRevLett.131.205002

Introduction.—Exploring the elementary processes driving the transformation of matter, such as photoemission delay [1], tunneling delay time [2], valence electron motion in atoms [3], charge migration [4], and proton dynamics [5] in molecules, urgently needs advanced techniques with attosecond temporal resolution and angstrom spatial resolution. The discovery of high-harmonic generation (HHG) [6–9] sets the basis for the generation of attosecond pulses and has opened the opportunity to investigate electronic ultrafast processes on the attosecond timescale. In parallel with the development of the HHG technique, the last decades have witnessed the rise of high-gain x-ray free-electron lasers (XFELs) that have unique advantages in producing ultrashort x-ray pulses with unprecedented peak brightness [10,11]. Various methods [12–20] based on XFELs have been proposed and demonstrated in recent years to further shorten the pulse duration to attosecond regime while maintaining the peak power at the tens of gigawatts level, complementing state-of-the-art HHG techniques with limited pulse energies at x-ray wavelengths. On the other hand, the characterization of temporal information of these ultrashort XFEL pulses is equally important, because precise knowledge of the spectrotemporal distribution is beneficial for ultrafast experiments designed to make full use of the laserlike properties of XFELs.

The temporal structure of XFEL pulses can be indirectly inferred by measuring the longitudinal phase space of the electron beam after lasing with an x-band radio frequency transverse deflector [21]. This method has been widely adopted by XFEL facilities and has achieved a temporal resolution of a few femtoseconds [22–24]. Direct experimental determinations of the temporal structures of FEL pulses have recently been accomplished by the terahertz- or laser-assisted streaking measurements with resolutions ranging from femtoseconds to hundreds of attoseconds [25–30]. The streaking spectroscopies are powerful techniques that can not only retrieve the time-energy structure of x-ray FEL pulses, but also provide new insights into the temporal jitter behavior, which is particularly important for FEL facilities. Additionally, several potential methods have been developed to characterize ultrafast EUV and x-ray pulses in conjunction with the frequency resolved optical gating or spectral phase interferometry for direct electric-field reconstruction (SPIDER) techniques [31–36]. However, these methods generally require the use of suitable nonlinear materials, which are not universal for different wavelengths and are generally lacking at short wavelengths. To overcome this problem, some attempts and efforts have been made to measure the spectrotemporal distributions of seeded FELs [37] or the electric-field waveform of the spontaneous radiation [38].

In this Letter, we propose a generally applicable method to retrieve the spectrotemporal properties of ultrashort FEL pulses. With an electron beam initiating coherent radiation successively in the main FEL amplifier and an afterburner, a pair of spectrally sheared pulses with an appropriate time delay could be produced, resulting in a self-referenced spectral interferogram (SSI) that can be used for single-shot

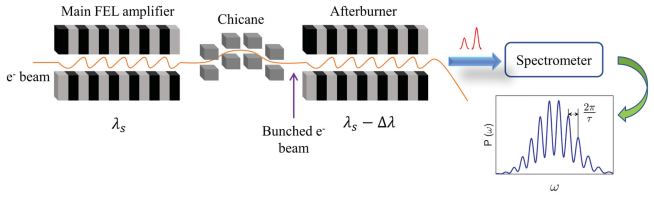

FIG. 1. Schematic layout of the proposed method.

reconstruction of the FEL pulses. Compared with other existing methods, this method combines the following advantages: it is simple and cost effective, noninvasive, applicable to any wavelength, and has higher resolutions for shorter FEL pulses. The proposed method is suitable for various ultrashort XFEL generation techniques either based on self-amplified spontaneous emission (SASE) or external seeding, and will open up a new area of attoscience with high intensity XFELs.

Methods and 3D numerical simulations.—The schematic layout of the proposed technique is shown in Fig. 1, where a small chicane and a short undulator (afterburner) have been added downstream of the main FEL amplifier. After generating an attosecond x-ray pulse (sample pulse) in the main amplifier, the electron beam with strong microbunching that formed in the main amplifier will initiate coherent radiation (reference pulse) in the following afterburner. The chicane is used to delay the electron beam and induce a temporal shift between these two radiation pulses. For a sufficiently homogeneous electron beam with constant energy in the lasing fraction, the attosecond pulses generated in the main amplifier and afterburner will have equal temporal phases that follow the distribution of the microbunchings. It is worth noting that the sample pulse cannot be acquired too far beyond the saturation, where the microbunching changes dramatically in a short distance. In the proposed method, the generation of a pair of frequency-sheared pulses is an imperative prerequisite for the phase retrieval procedure. The required slight frequency shift can be induced by the frequency-pulling effect, when a mismatch between the frequency of the microbunching and the resonance of the undulator exists in the afterburner [39]. The wavelength shift can be calculated by

$$\Delta\lambda = \Delta\lambda_u \sigma_b^2/(\sigma_b^2 + \sigma_u^2). \quad (1)$$

Where λ_u is the undulator resonance wavelength, σ_b and σ_u are the FWHM bandwidths of the microbunching and gain spectra of the afterburner, respectively. The frequency-pulling effect described in Eq. (1) has also been demonstrated by simulations (see Supplemental Material [40]).

To investigate the performance of the proposed method, three-dimensional simulations with GENESIS1.3 [41] have been performed with realistic parameters of the Shanghai soft x-ray FEL facility (SXFEL) [42], as listed in Table I.

TABLE I. Main parameters of the SXFEL.

Parameters	Value	Unit
Electron beam energy	1.5	GeV
Peak current	800	A
Normalized emittance	0.65	mm mrad
Slice energy spread	150	keV
Main undulator period	1.6	cm

Based on the method in Ref. [17], attosecond soft x-ray pulses with the central wavelength λ_s of 2 nm, peak power of 282 MW, and pulse duration of 610 asec, were generated in the main undulator with period of 1.6 cm and K value of 1.1565, as shown in Fig. 2(a). The longitudinal space charge effect has been taken into account in the simulations, as what we have done in Ref. [43]. The saturation power was relatively low due to the limitations of the SXFEL electron beam parameters. After that, the bunched electron beams were sent through a small chicane with a dispersion strength of $R_{56} \approx 0.9$ μm to introduce a time delay of $\tau = 1.5$ fs. Simulation results show that this dispersion has little influence on the microbunchings in the electron beams, where the maximal bunching factor changes from 0.33 to 0.35. Then the electron beam travels through a short afterburner with period of 1.6 cm (same as the main undulator) and length of 0.304 m. The K value of the afterburner was tuned to 1.1559 to slightly shift the central frequency by $\Omega = 3 \times 10^{14}$ rad/s. A reference pulse with peak power of 92 MW and pulse duration of 560 asec has been generated, as shown in Fig. 2(a). The intensity difference between the sample pulse and the reference pulse usually exists, but it is not a critical factor

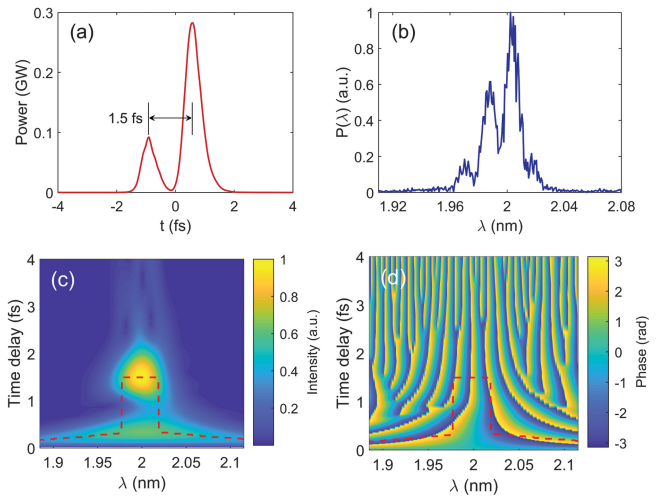

FIG. 2. Simulation and data analysis processes for the proposed method. (a) The temporal profiles of the sample pulse (right) and reference pulse (left). (b) The spectral shearing interferogram of these frequency-sheared pulses. Time-frequency magnitude topography (c) and phase topography (d) after WT.

for this method, as long as they are within the same order of magnitude (see Supplemental Material [40]). Figure 2(b) shows the eventual SSI of these two frequency-sheared pulses.

The next step is to extract the phase information from the SSI. Assuming the FEL pulse with an electric field $\tilde{E}(\omega) = |\tilde{E}(\omega)| \exp[i\phi(\omega)]$, the SSI function will take the following form:

$$S(\omega,\tau) = |\tilde{E}(\omega)|^2 + |\tilde{E}(\omega+\Omega)|^2 + 2|\tilde{E}(\omega)||\tilde{E}(\omega+\Omega)|\cos[\phi(\omega) - \phi(\omega+\Omega) + \omega\tau], \quad (2)$$

where Ω is the frequency shift and τ is the time delay between two pulses. For a structured spectrum, SPIDER takes on uncertainties for different filter widths [44]. To overcome this problem, the wavelet-transform (WT) algorithm had been proposed to extract the spectral phase instead of the Fourier-transform algorithm [44,45]. As a signal analysis tool, the WT technique has great advantages in analyzing signals with complicated frequency components. The WT of SSI function $S(\omega')$ can be expressed as

$$W(\Delta\omega,\omega) = \frac{1}{\Delta\omega}\int_{-\infty}^{+\infty} S(\omega')\psi^*\left(\frac{\omega'-\omega}{\Delta\omega}\right)d\omega', \quad (3)$$

where $\psi[(\omega'-\omega)/\Delta\omega]$ is the daughter wavelet generated by dilation and translation of the Gabor mother wavelet $\psi(\omega) = e^{(-\omega^2/2\sigma^2+i2\pi\omega)}/(\sigma^2\pi)^{1/4}$ (here $\sigma = 1/\sqrt{2\ln 2}$). Based on this method, the shaping factor of the Gabor wavelet has little effect on the phase retrieval [44]. According to the relationship between τ and fringe spacing $\Delta\omega$ of the shearing interferogram, i.e., $\tau = 2\pi/\Delta\omega$, Eq. (3) can be written as another form:

$$W(t,\omega) = \frac{t}{2\pi}\int_{-\infty}^{+\infty} S(\omega')\psi^*\left[\frac{(\omega'-\omega)\cdot t}{2\pi}\right]d\omega'. \quad (4)$$

After performing the WT of $S(\omega,\tau)$, a one-dimensional frequency domain SSI signal is converted into two time-frequency graphics in Figs. 2(c) and 2(d): the magnitude topography and phase topography, reflecting the intensity and phase information in the time-frequency plane, respectively. We search for the maximum value of the magnitude topography at each frequency point, i.e., the red ridge curve in Fig. 2(c), and then project it onto the phase topography, from which the phase $\phi(\omega) - \phi(\omega+\Omega) + \omega\tau$ can be extracted directly. The linear term $\omega\tau$ can be removed utilizing the time delay τ read from Fig. 2(c). And then the spectral phase $\phi(\omega)$ can be retrieved through an inversion routine [34]. The WT algorithm avoids the influence of phase noise as much as possible since the phase along the maximum value of the magnitude topography is extracted from the phase topography. The spectra of sample and reference pulses can also be recovered from the interferogram (see Supplemental Material [40]). Assuming $S_1(\omega) = |\tilde{E}(\omega)|^2 + |\tilde{E}(\omega+\Omega)|^2$, $S_2(\omega) = 2|\tilde{E}(\omega)||\tilde{E}(\omega+\Omega)|$, the spectral intensity $|\tilde{E}_{\rm sam}(\omega)|$ and $|\tilde{E}_{\rm ref}(\omega)|$ can be expressed as

$$|\tilde{E}_{\rm sam}(\omega)| = \frac{1}{2}[\sqrt{S_1(\omega)+S_2(\omega)} + \sqrt{S_1(\omega)-S_2(\omega)}],$$
$$|\tilde{E}_{\rm ref}(\omega)| = \frac{1}{2}[\sqrt{S_1(\omega)+S_2(\omega)} - \sqrt{S_1(\omega)-S_2(\omega)}]. \quad (5)$$

With the above method, the spectrum and the retrieved spectral phase were obtained and given in Fig. 3(a). After the Fourier transform, the reconstructed temporal profile and phase are present in Fig. 3(b) (red lines). The duration of reconstructed pulse is about 590 asec, fitting well with the initial pulse duration of 610 asec exported from GENESIS (blue lines). In order to verify the stability of the proposed method, multishot simulations have also been performed by varying the initial stochastic noise of the electron beams. Simulation results are summarized in Fig. 3(c). The reconstruction error of the pulse duration is calculated to be about 5.6% (rms), which is acceptable for the pulse characterization. The error can be reduced by increasing τ to create more interference fringes. However, τ has an upper limit determined by the R_{56} so that the

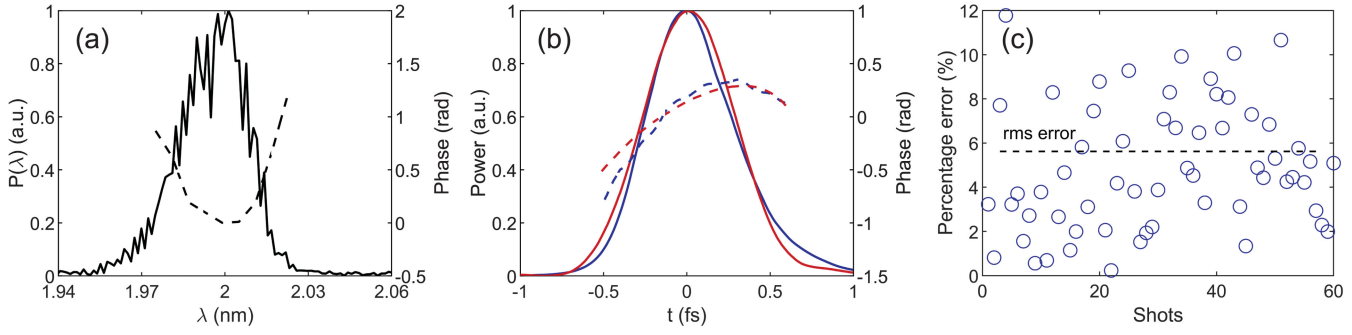

FIG. 3. Spectrotemporal reconstructions of attosecond pulses. (a) Spectrum (solid line) and retrieved spectral phase (dashed line). (b) Temporal profiles and phases of the reconstructed pulse (red) and that directly exported from simulation (blue). (c) Statistical analysis of the reconstructed pulse duration for multishot simulations (60 shots).

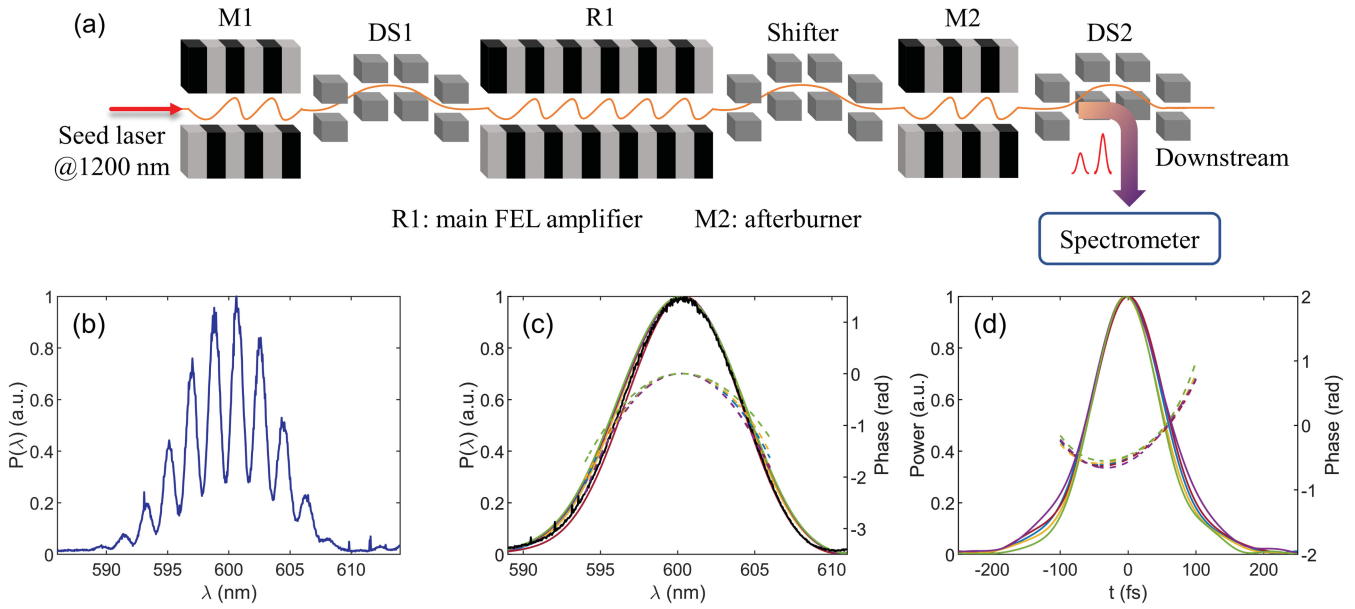

FIG. 4. Experimental layout and results. (a) Layout of the proof-of-principle experiment for the proposed method. (b) Typical spectral shearing interferogram. (c) Directly measured spectrum (black solid line), reconstructed spectra (color solid lines), and spectral phases (color dashed lines) obtained from five consecutive FEL shots. (d) Reconstructed temporal profiles (solid lines) and phases (dashed lines) obtained from five consecutive FEL shots. Lines of the same color represent the same FEL pulse.

bunching is not blurred after the chicane, i.e., $R_{56} < \gamma\lambda_s/2\pi\sigma_\gamma$ [46]. Therefore, for shorter pulse durations, the precision of the proposed method will improve due to the larger bandwidths (more fringes).

Experiment.—The feasibility of the proposed method has been demonstrated using the experimental data measured at the Shanghai Deep Ultraviolet Free Electron Laser test facility (SDUV-FEL) [47–49]. During the experiments, the facility was operated with the high-gain harmonic generation (HGHG) mode [49], as shown in Fig. 4(a). Comparing with SASE, HGHG can produce FEL pulses with stable and repeatable properties, providing ideal conditions for testing the feasibility and reproducibility of the proposed method. A 148 MeV electron beam with bunch charge of 200 pC and bunch length of about 8.8 ps interacts with a 1200 nm seed laser pulse with a duration of about 150 fs (FWHM) in the modulator (M1) with a period length of 50 mm and total length of 0.5 m to generate coherent energy modulation. After passing through a dispersive chicane (DS1) to convert the energy modulation into microbunching, the electron beam is sent into the radiator (R1) with a period length of 40 mm and total length of 1.6 m to generate a FEL pulse (sample pulse) at 600 nm (second harmonic) with the temporal properties similar to the seed laser. The electron beam then consecutively passages through a small chicane (shifter) to induce a time delay of 600 fs and an afterburner (M2) with period length of 40 mm and total length of 0.64 m to produce the reference pulse. The resonance condition of M2 was tuned to shift the central wavelength of the reference pulse by $\Delta\lambda = 0.55$ nm, which corresponds to a frequency shift of $\Omega \approx 2.88 \times 10^{12}$ rad/s. The SSI signal was measured by a spectrometer (TRIAX-550, Jobin Yvon) downstream of the afterburner.

Figure 4(b) shows a typical single-shot interferogram detected by the spectrometer, which is consistent with the theoretical simulations (see Supplemental Material [40]). With the proposed method, Figs. 4(c) and 4(d) show the reconstruction results in the spectral and temporal domains for five consecutive FEL shots. The retrieved phases and longitudinal profiles are consistent with each other, demonstrating the reproducibility of the proposed method. The spectral envelopes (color solid lines) calculated by Eq. (5) match well with the directly measured single-shot spectrum (black solid line). The retrieved temporal phase profiles have similar curvatures that reflect the positive frequency chirp in the seed laser. The average spectral bandwidth and pulse duration of the reconstructed pulses are 8.9 nm and 175 fs (FWHM), respectively, in accordance with the theoretical predictions considering the slippage effect in the radiator. The fluctuation of the retrieved pulse duration is less than 6%.

Conclusion.—In conclusion, we have proposed and demonstrated a novel and feasible diagnostic method that can fully characterize the spectrotemporal information of the ultrashort FEL pulse on a single-shot basis. By performing a wavelet transform of the spectral shearing interferogram, one can retrieve the spectral phase and reconstruct the FEL pulse with attosecond resolution. The proposed method can be easily implemented in current XFEL facilities by adding a small chicane between the last two undulator segments of the FEL amplifier, making the

last undulator work as the afterburner and using an on-line spectrometer to detect the SSI signal. To avoid affecting user experiments, one could use the quadrupole before the afterburner to kick the electron beam with a tiny angle, which would spatially separate the sample and reference pulses after a long distance [40,50]. This would enable blocking the reference pulse after detection and eliminate its interference with user experiments. Furthermore, this method has the potential to be generalized to cases where ultrashort radiation pulses have multiple spikes [40]. This method would enable us to tune the machine for generating custom-tailored FEL pulses and explore new possibilities of attosecond science with x-ray attosecond pump-probe techniques.

This work was supported by the National Natural Science Foundation of China (12122514, 11975300) and the Shanghai Science and Technology Committee Rising-Star Program (20QA1410100).

*fengc@sari.ac.cn

[1] M. Schultze *et al.*, Science **328**, 1658 (2010).
[2] P. Eckle, A. N. Pfeiffer, C. Cirelli, A. Staudte, R. Dorner, H. G. Muller, M. Buttiker, and U. Keller, Science **322**, 1525 (2008).
[3] E. Goulielmakis, Z.-H. Loh, A. Wirth, R. Santra, N. Rohringer, V. S. Yakovlev, S. Zherebtsov, T. Pfeifer, A. M. Azzeer, M. F. Kling, S. R. Leone, and F. Krausz, Nature (London) **466**, 739 (2010).
[4] P. M. Kraus, B. Mignolet, D. Baykusheva, A. Rupenyan, L. Horný, E. F. Penka, G. Grassi, O. I. Tolstikhin, J. Schneider, F. Jensen, L. B. Madsen, A. D. Bandrauk, F. Remacle, and H. J. Wörner, Science **350**, 790 (2015).
[5] S. Baker, J. S. Robinson, C. A. Haworth, H. Teng, R. A. Smith, C. C. ChirilA, M. Lein, J. W. G. Tisch, and J. P. Marangos, Science **312**, 424 (2006).
[6] M. Hentschel, R. Kienberger, C. Spielmann, G. A. Reider, N. Milosevic, T. Brabec, P. Corkum, U. Heinzmann, M. Drescher, and F. Krausz, Nature (London) **414**, 509 (2001).
[7] H. Vincenti and F. Quéré, Phys. Rev. Lett. **108**, 113904 (2012).
[8] J. Li, J. Lu, A. Chew, S. Han, J. Li, Y. Wu, H. Wang, S. Ghimire, and Z. Chang, Nat. Commun. **11**, 2748 (2020).
[9] E. J. Takahashi, T. Kanai, K. L. Ishikawa, Y. Nabekawa, and K. Midorikawa, Phys. Rev. Lett. **101**, 253901 (2008).
[10] P. Emma *et al.*, Nat. Photonics **4**, 641 (2010).
[11] E. Allaria *et al.*, Nat. Photonics **7**, 913 (2013).
[12] A. A. Zholents, Phys. Rev. ST Accel. Beams **8**, 040701 (2005).
[13] J. Duris, S. Li, T. Driver, E. G. Champenois, J. P. MacArthur, A. A. Lutman, Z. Zhang, P. Rosenberger, J. W. Aldrich, R. Coffee, G. Coslovich, and F.-J. Decker, Nat. Photonics **14**, 30 (2020).
[14] Z. Wang, C. Feng, and Z. Zhao, Phys. Rev. Accel. Beams **20**, 040701 (2017).
[15] Z. Qi, C. Feng, H. Deng, B. Liu, and Z. Zhao, Phys. Rev. Accel. Beams **21**, 120703 (2018).
[16] Y. Xiao, C. Feng, and B. Liu, Ultrafast Science (2022). 10.34133/2022/9812478
[17] L. Tu, Z. Qi, Z. Wang, S. Zhao, Y. Lu, W. Fan, H. Sun, X. Wang, C. Feng, and Z. Zhao, Appl. Sci. **12**, 11850 (2022).
[18] D. Xiang, Z. Huang, and G. Stupakov, Phys. Rev. ST Accel. Beams **12**, 060701 (2009).
[19] T. Tanaka, Phys. Rev. Lett. **114**, 044801 (2015).
[20] C. Feng, J. Chen, and Z. Zhao, Phys. Rev. ST Accel. Beams **15**, 080703 (2012).
[21] Y. Ding, C. Behrens, P. Emma, J. Frisch, Z. Huang, H. Loos, P. Krejcik, and M.-H. Wang, Phys. Rev. ST Accel. Beams **14**, 120701 (2011).
[22] C. Behrens, F. J. Decker, Y. Ding, V. A. Dolgashev, J. Frisch, Z. Huang, P. Krejcik, H. Loos, A. Lutman, T. J. Maxwell, J. Turner, J. Wang, M. H. Wang, J. Welch, and J. Wu, Nat. Commun. **5**, 3762 (2014).
[23] C. Feng *et al.*, Optica **9**, 785 (2022).
[24] E. Allaria, G. De Ninno, S. Di Mitri, W. M. Fawley, E. Ferrari, L. Fröhlich, G. Penco, P. Sigalotti, S. Spampinati, C. Spezzani, and M. Trovò, Phys. Rev. ST Accel. Beams **17**, 010704 (2014).
[25] P. Radcliffe, S. Düsterer, A. Azima, H. Redlin, J. Feldhaus, J. Dardis, K. Kavanagh, H. Luna, J. P. Gutierrez, P. Yeates, E. T. Kennedy, J. T. Costello, A. Delserieys, C. L. Lewis, R. Taïeb, A. Maquet, D. Cubaynes, and M. Meyer, Appl. Phys. Lett. **90**, 131108 (2007).
[26] V. S. Yakovlev, J. Gagnon, N. Karpowicz, and F. Krausz, Phys. Rev. Lett. **105**, 073001 (2010).
[27] W. Helml *et al.*, Nat. Photonics **8**, 950 (2014).
[28] I. Grguraš, A. R. Maier, C. Behrens, T. Mazza, T. J. Kelly, P. Radcliffe, S. Düsterer, A. K. Kazansky, N. M. Kabachnik, T. Tschentscher, J. T. Costello, M. Meyer, M. C. Hoffmann, H. Schlarb, and A. L. Cavalieri, Nat. Photonics **6**, 852 (2012).
[29] N. Hartmann *et al.*, Nat. Photonics **12**, 215 (2018).
[30] D. C. Haynes *et al.*, Nat. Phys. **17**, 512 (2021).
[31] M. Lucchini and M. Nisoli, Appl. Sci. **8** (2018).
[32] M. Lucchini, M. Brügmann, A. Ludwig, L. Gallmann, U. Keller, and T. Feurer, Opt. Express **23**, 29502 (2015).
[33] W. K. Peters, T. Jones, A. Efimov, E. Pedersoli, L. Foglia, R. Mincigrucci, I. Nikolov, R. Trebino, M. B. Danailov, F. Capotondi, F. Bencivenga, and P. Bowlan, Optica **8**, 545 (2021).
[34] C. Iaconis and I. Walmsley, IEEE J. Quantum Electron. **35**, 501 (1999).
[35] M. Anderson, L. de Araujo, E. Kosik, and I. Walmsley, Appl. Phys. B **70**, S85 (2000).
[36] S. Jensen and M. E. Anderson, Appl. Opt. **43**, 883 (2004).
[37] G. D. Ninno, D. Gauthier, B. Mahieu, P. R. Ribič, E. Allaria, P. Cinquegrana, M. B. Danailov, A. Demidovich, E. Ferrari, L. Giannessi, G. Penco, P. Sigalotti, and M. Stupar, Nat. Commun. **6**, 8075 (2015).
[38] T. Fuji, T. Kaneyasu, M. Fujimoto, Y. Okano, E. Salehi, M. Hosaka, Y. Takashima, A. Mano, Y. Hikosaka, S.-i. Wada *et al.*, Optica **10**, 302 (2023).
[39] E. Allaria, G. D. Ninno, and C. Spezzani, Opt. Express **19**, 10619 (2011).
[40] See Supplemental Material at http://link.aps.org/supplemental/10.1103/PhysRevLett.131.205002 for theoretical simulation of the proof-of-principle experiment.
[41] S. Reiche, Nucl. Instrum. Methods Phys. Res., Sect. A **429**, 243 (1999).

[42] B. Liu, C. Feng, D. Gu, F. Gao, H. Deng, M. Zhang, S. Sun, S. Chen, W. Zhang, W. Fang, Z. Wang, Q. Zhou, Y. Leng, M. Gu, L. Yin, Q. Gu, G. Fang, D. Wang, and Z. Zhao, Appl. Sci. (Switzerland) **12**, 176 (2022).
[43] Z. Wang and C. Feng, High Power Laser Sci. Eng. **11**, e33 (2023).
[44] Y. Deng, Z. Wu, S. Cao, L. Chai, C. yue Wang, and Z. Zhang, Opt. Commun. **268**, 1 (2006).
[45] Y. Deng, Z. Wu, L. Chai, C. yue Wang, K. Yamane, R. Morita, M. Yamashita, and Z. Zhang, Opt. Express **13**, 2120 (2005).
[46] E. A. Schneidmiller, Phys. Rev. Accel. Beams **25**, 010701 (2022).
[47] B. Liu, W. Li, J. Chen, Z. Chen, H. Deng, J. Ding, Y. Fan, G. Fang, C. Feng, L. Feng *et al.*, Phys. Rev. ST Accel. Beams **16**, 020704 (2013).
[48] Z. T. Zhao *et al.*, Nat. Photonics **6**, 360 (2012).
[49] C. Feng, M. Zhang, G. Q. Lin, Q. Gu, H. X. Deng, J. H. Chen, D. Wang, and Z. T. Zhao, Chin. Sci. Bull. **57**, 3423 (2012).
[50] J. P. MacArthur, A. A. Lutman, J. Krzywinski, and Z. Huang, Phys. Rev. X **8**, 041036 (2018).